Tailoring Coherent Beam Combined laser pulse train for high peak and average power applications

Claude-Alban Ranély-Vergé-Dépré, Corentin Lechevalier, Jordan Andrieu, Ihsan Fsaifes, Igor Jovanovic, Jean-Christophe Chanteloup

Tailoring Coherent Beam Combined Laser Pulse Train for High Peak and Average Power Applications

Claude-Alban Ranély-Vergé-Dépré[1,2], Corentin Lechevalier[1], Jordan Andrieu[1], Ihsan Fsaifes[1], Igor Jovanovic[3], and Jean-Christophe Chanteloup [1]

[1] *LULI, CNRS, École Polytechnique, CEA, Sorbonne Université, Institut Polytechnique de Paris, 91120 Palaiseau, France*

[2] *Thales LAS France SAS, 2 avenue Gay Lussac, 78995 Elancourt, France*

[3] *Gérard Mourou Center for Ultrafast Optical Science, University of Michigan, Ann Arbor, MI 48109, USA*

Abstract Laser systems based on Coherent Beam Combination (CBC) that rely on the tiled pupil architecture intrinsically carry digital capabilities independently applicable to all three essential characteristics of a laser pulse: amplitude, phase, and polarization. Those capabilities allow the far-field energy distribution to be flexibly tailored in real time. Operation in the femtosecond regime at high repetition rates gives access to a wide range of applications requiring both high peak and average powers. We address the task of independent peak versus average power adjustment needed for applications seeking to decouple nonlinear phenomena associated with GW peak power from the thermal load inherent to kW average power operation. The technical solutions proposed are presented in the framework of the Ecole Polytechnique XCAN CBC laser platform (61 independent channels) with an emphasis on thermal management measures implemented to ensure its nominal operation.

Key words: Laser power management, optical chopper, laser on demand, digital laser, coherent beam combination

INTRODUCTION

Optimizing laser systems to produce high average or high peak power for serving high-power laser users and applications is a Cornelian choice that has been largely superseded by recent technical progress made in laser amplifier design. C. Saraceno *et al.* (Fig. 1 in Ref. [1]) highlight that the average power ~kW limit for pulsed lasers is now surpassed by lasers based on three major amplifier geometries: slabs, disks, and fibers. Among these, fiber optics offer the greatest potential in terms of scalability. Their mechanical flexibility and large heat exchange surface make them indeed ideal candidates for innovative architectures like those required for Coherent Beam Combination (CBC), where many amplifiers produce parallel beams in a limited volume [2]. In the kW average power regime, the wall plug efficiency η_{wp} becomes a crucial parameter. Thanks to efficient laser diodes (η_{wp}>50–70%), pump losses have been dramatically reduced in recently developed fiber amplifiers. Selecting an optimal doping ion (Yb^{3+}, Er^{3+}, Tm^{3+}, ...) to be hosted in the silica matrix of an optical fiber also contributes to improved efficiency. With a quantum efficiency of η_q=94%, it is no surprise that Yb-doped optical fiber is the building block of choice for fiber lasers and especially CBC laser systems.

The rise in average power is intrinsically linked to and limited by the overall efficiency of laser systems and the associated thermal management. We provide an overview of technical solutions implemented on the Ecole Polytechnique XCAN digital CBC laser to achieve efficient thermal management and address the users' need to independently adjust the peak and average power. Such tailoring of laser output is a crucial part of the laser's evolution towards a versatile user platform. The digital aspect conferred by individual control of amplitude and phase [3] and recent developments in polarization control [4] is one essential aspect of this. The XCAN amplification section resides within the chirped-pulse amplification (CPA) architecture such that the seed pulse is split after stretching, and the split amplified channels are recombined into a single beam before compression. Thanks to a cascaded chirped fiber Bragg grating (CFBG) stretcher and post-compression, XCAN offers a wide range of pulse durations. The stretcher relies on twelve CFBG fibers allowing 416 ps of stretching each, resulting in 13 distinct pulse durations between 0.4 and 5 ns. A standard reflective grating pair compressor reduces the pulse duration to ~300 fs, while a subsequent nonlinear post-compression stage [5] leads to 60 fs output. Independent control of average and peak power also contributes to system versatility, offering full spatial, temporal, vectorial, energetic, and power control to users.

While section 1 illustrates water cooled solutions implemented at the amplifier and laser head level and present CBC far fields recorded with such thermal management approaches, section 2 summarized water-cooled pinhole material studies. Finally, section 3 explains how independent control of average and peak powers can be achieved through the combined use of a fast spinning mirror and a water-cooled Pockels cell. The schematic diagram of figure 1 helps visualizing where and how the proposed technical solutions are implemented within the laser system.

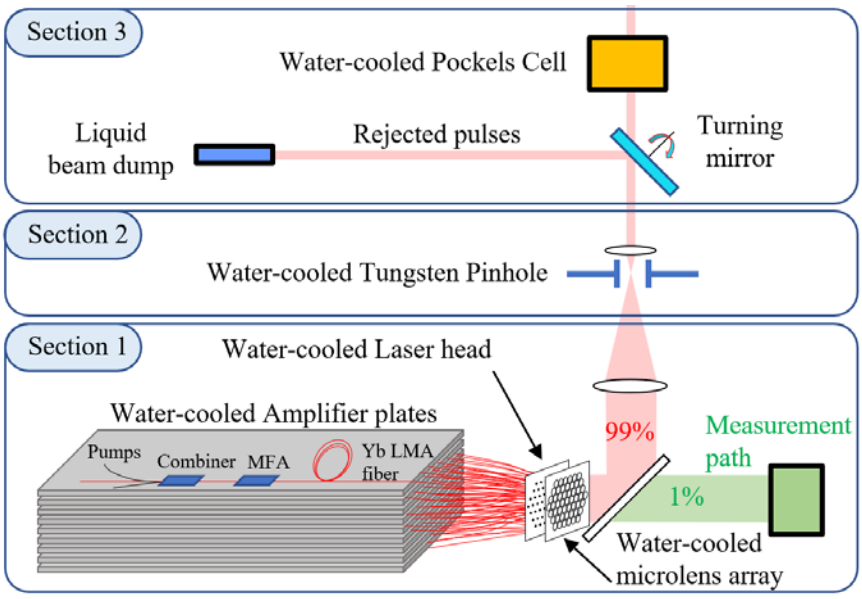

Figure 1. Schematic diagram of the laser system amplifier and free space propagation. Subjects of sections 1, 2 and 3 of this paper are identified from bottom to top. The 61 amplifying fiber are represented in red coming out from a set of 9 cooled plate between which they are distributed before converging to form a bundle within the laser head (section 1). Whereas a small fraction (in green) of the light is diverted towards a measurement path dedicated at servo loop control for CBC, the main beam (in red) undergoes a spatial selection (section 2) followed by a temporal selection within the pulse train (section 3).

EXPERIMENTAL IMPLEMENTATIONS AND DEVELOPMENTS

1. Amplifier and Laser Head

The 61 amplifying stages key elements (combiners, mode field adaptors (MFA) and large mode area (LMA) fibers [2]) rest on a set of 9 aluminum plate actively cooled through water circulating into built-in copper duct (top of fig. 2b&c). Without water cooling, temperatures as high as 75°C were recorded while it is limited to about 25°C maximum (see fig 4) with flowing coolant. More aggressive thermal management had to be implemented at the laser head that contains 61 fiber amplifier outputs (Figure 2) with up to 25 W of pulsed extracted light at 1030 nm and up to 1 W of unabsorbed CW pump light at 976 nm per channel. For all channels, this sum up to 1.5 kW total average power over a 6.5 cm^2 transverse section of the laser head where the fiber-to-fiber pitch is 3.2 mm. Ensuring highly stable individual beam position and pointing accuracy (µm and mrad scale, respectively) at this stage is mandatory for an efficient CBC [6].

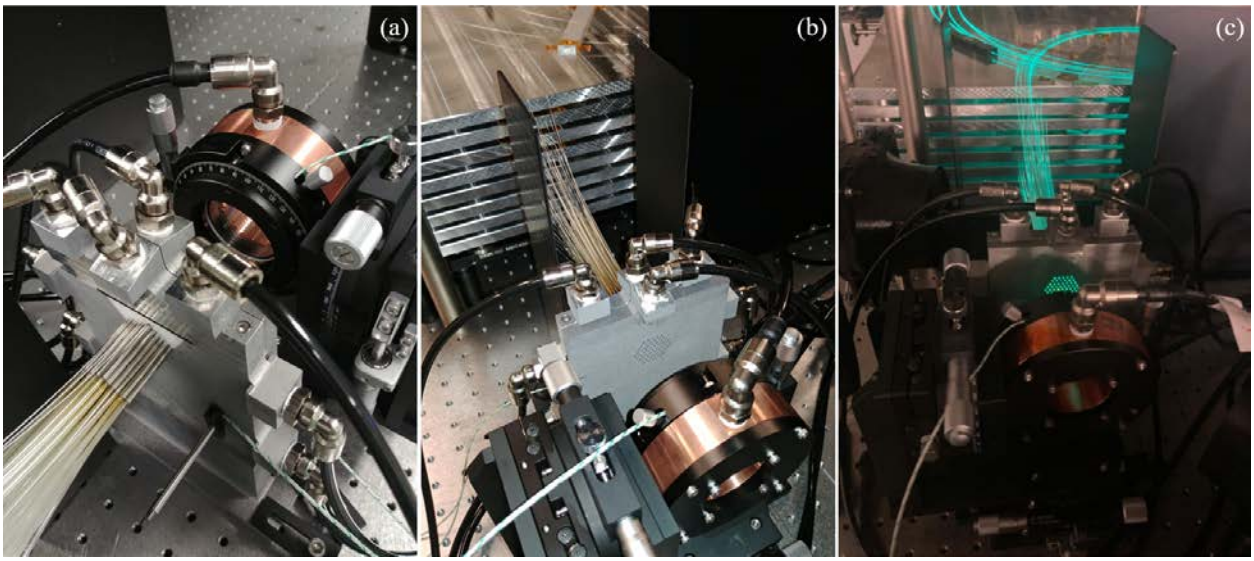

Figure 2. 3D printed water-cooled laser head hosting sleeves (white zirconium cylinder) in a V-shaped holder. Ferule-equipped fiber ends are inserted into the sleeves for accurate alignment. Downstream the laser head, the water-cooled copper microlens array mount can be seen while upstream the laser head, the 9 water-cooled fiber amplifier supporting plates can be observed. (a) Back side and (b) front side views; (c) front side with Yb-doped fiber fluorescence.

Most of the optical mounts along the subsequent beam path, including those that contain the collimated microlens array, 2-inch lens, and mirrors, are water cooled as well.

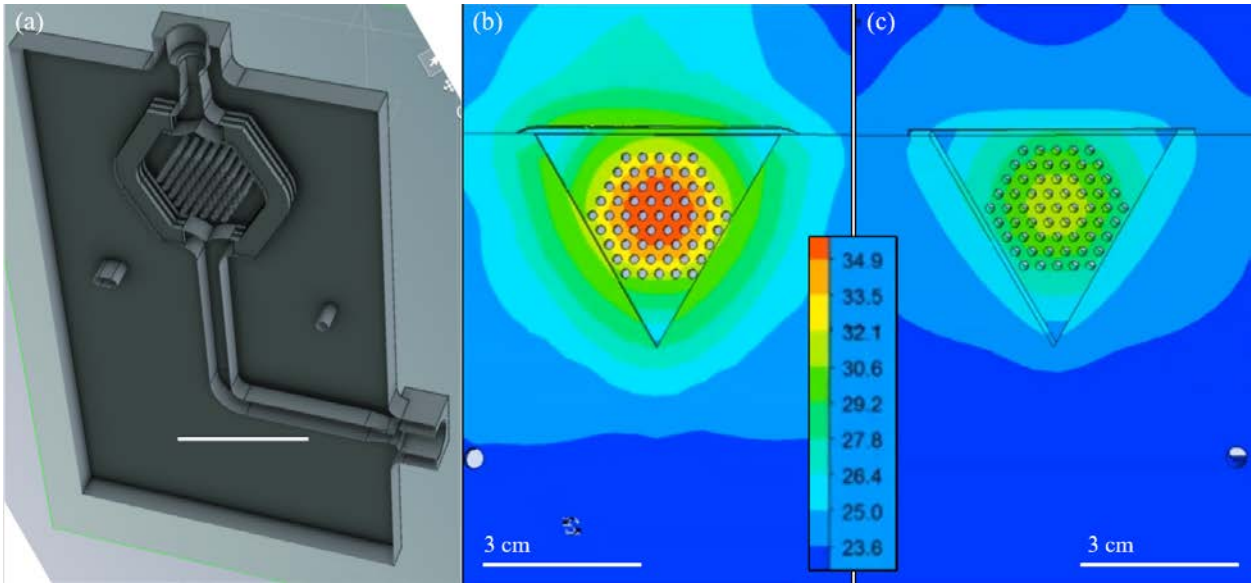

Figure 3. CAD view of the 61-hole plate collecting the unabsorbed 976 nm CW pump light refracted through the fiber end-cap (a). The cooling channel is split into two subchannels to maximize surface exchange and optimize heat removal. Thermal modeling shows a 14°C thermal gradient for single-channel cooling ducts (b) while it reveals a 10°C thermal gradient for split channel cooling ducts (c). A heat source of approximately 1 W per hole was considered in the model.

Such a holistic and proactive approach to thermal management is needed since the final combined single beam stability is crucial for subsequent laser stages to perform adequately: stability affects central lobe pinhole selection centering, chopper/Pockels cell (see Section 3) power management

stage tailoring, alignment of compressor and post-compression cells [7], frequency conversion, and final focusing. Together, these measures limit the beam deviation to about 10% of its diameter. The laser head is an optomechanical assembly that poses most severe demands on the heat management. It consists of 3D-printed aluminum elements carefully adjusted with respect to each other. Thanks to metal additive manufacturing it is possible to internally structure the cooling ducts to maximize the heat exchange coefficient for optimum thermal load removal. Figure 3 shows an internal CAD view of the split duct that reduces the thermal gradient by ~30%.

Respective cooling efficiencies at an amplifier plate and the laser head level can be compared on figure 4 where far fields recorded in the pinhole plane are displayed. At t=8 minutes the CW diode pump operating current was instantaneously increased from 2 to 5A bringing the total optical power from 67W to bout 450W. While the laser head gets thermally stabilized within one minute, it takes about an hour for the amplifier plate. The temperature amplitude variation is really weak, especially when compared with the previous 75°C reached without water-cooling of the plates.

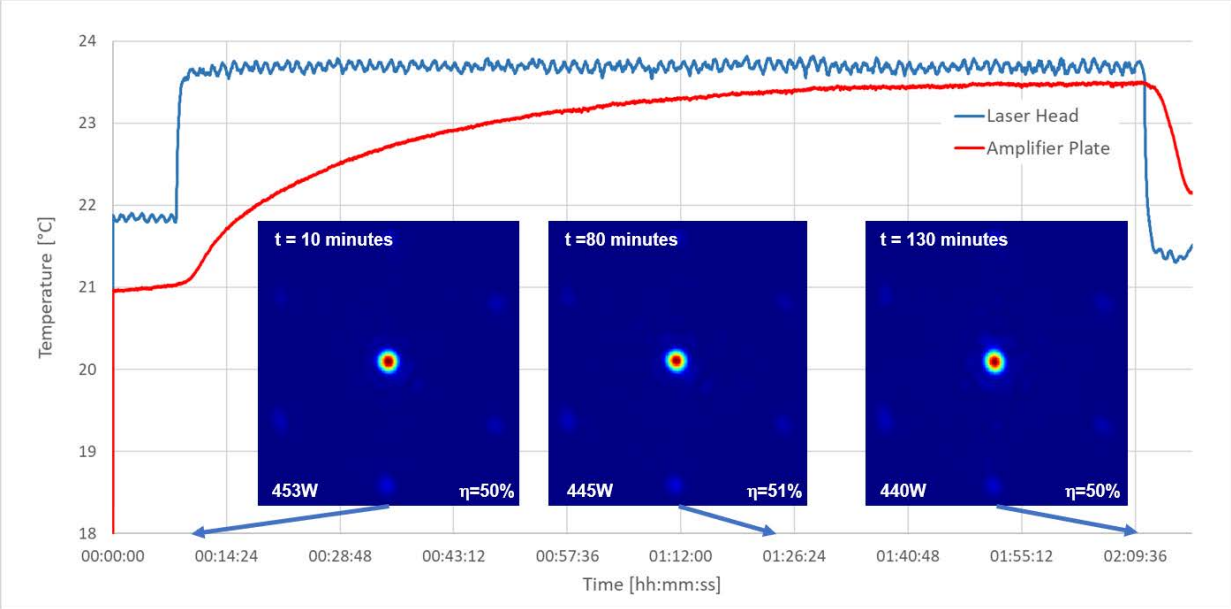

Figure 4. Temperature evolution over a 2 hours period recorded through PT100 thermal probes fixed at an amplifier plate (red) and the laser head (blue). Far fields recorded in the pinhole plane are displayed a t=10, 80 and 130 minutes. The pump was set at 5A a t=8 minutes. Repetition rate is 55 MHz and a 50% stable efficiency is recorded, leading to a ~220W average power beam after the pinhole.

Figure 5 (top 3 images) reveals a 7% drop in efficiency when operating at the kW level (pump diode operating current set at 8.6A) with a stable 43% value over an hour period (at 55 MHz repetition rate). Amplifier plates and laser head temperatures (not displayed) stabilized respectively at 24.1°C and 24.4°C, i.e. less than a degree above the temperatures recorded at half this average power (figure 4). Bottom 3 images are recorded with decreasing repetition rates (55, 1 and 0.5 MHz) allowing the energy per pulse to increase up to ~1 mJ in the central lobe. Operation at such energy level means a rather strong non-linear regime with an estimated B-integral level above 3 radians. It is likely to explain the extra 5% drop observed on the efficiency. After the pinhole a 400W average power pulse train is sent towards the compressor (~80% transmission) to reach 2.1 GW peak power (350 fs pulse duration).

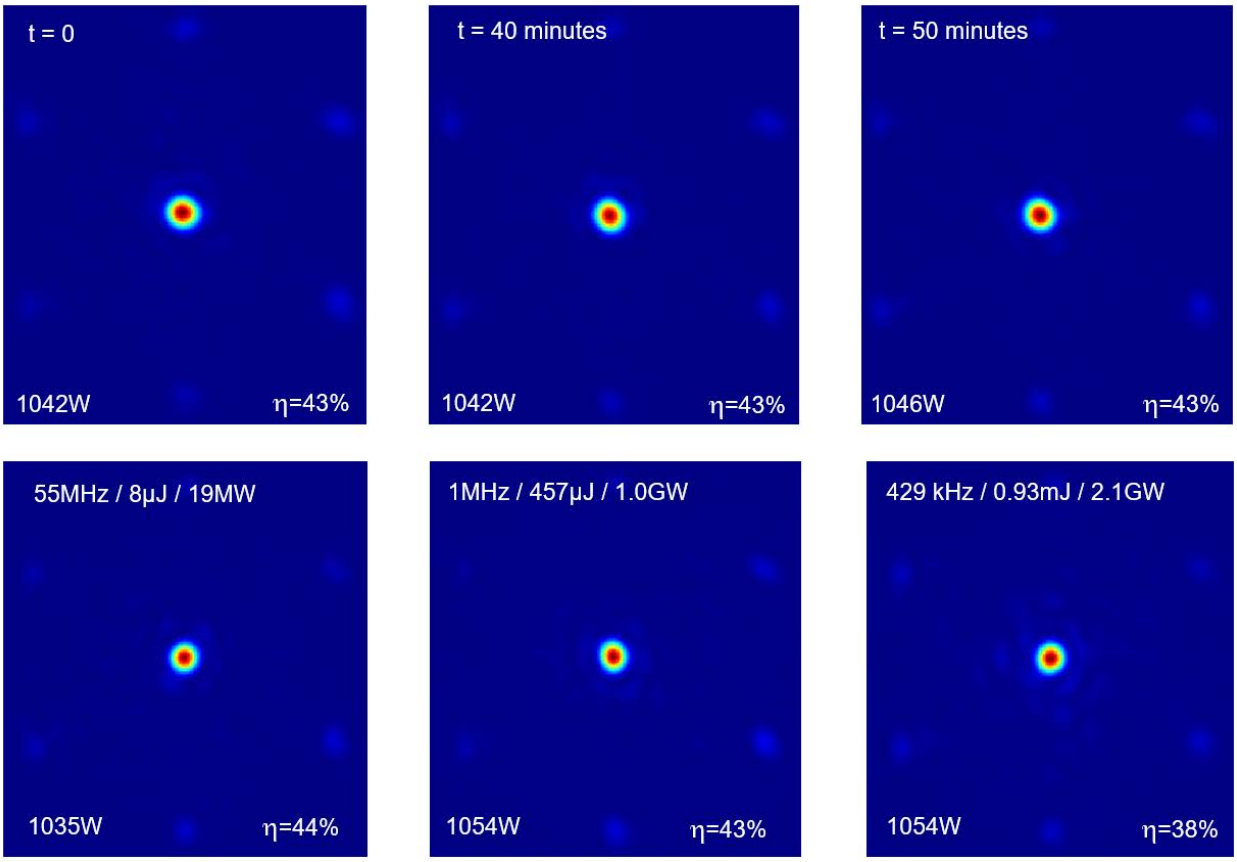

Figure 5. Far fields recorded in the pinhole plane in kW average power regime (bottom left values). The top 3 images are obtained at a 55 MHz repetition rate over a 50 minutes period. The bottom 3 images are obtained at a 55 MHz, 1MHz and 429kHz repetition rates. Energy in the main lobe is given as well as peak power after compression at 350 fs.

2. Central lobe selection

XCAN laser relies on 61 Yb-doped Large Mode Area (LMA) fiber amplifiers combined in a tiled aperture architecture (also known as far-field combining). CBC is performed with the help of a single optics: a large (2 inch) aperture lens that collects all sixty-one 3.2 mm-spaced adjacent sub pupils. At the lens focal plane, the central lobe theoretically concentrates up to 66% of the total power. The remaining power is distributed mainly into six surrounding lobes, carrying about 5% of the total power each. In practice, around 50% of the energy is contained in the central lobe, a value that can decrease to 40% when operating in the kW average power regime; and a non-negligible amount of power lies in a diffuse speckle between the central and the six surroundings lobes. A pinhole is placed in the focal plane to block the speckle light and deliver a clean TEM00 beam to users.

To maintain the pinhole integrity over long operation time, it is placed in a water-cooled mount. Then, one needs to make sure it is made of a material able to sustain high average power delivered in the nanosecond regime. Finally, one has to make sure the surrounding lobes are not focusing outside the pinhole. Several materials were tested: stainless steel (316L), tungsten-lanthanum oxide (WL10), and zirconium oxide (ZrO_2) with respective fusion temperatures of 1400°C, 2715°C. and 3420°C. Whereas the stainless-steel pinhole started melting quickly (at 440 W

average power level, see Figure 6 (a)), no degradation of the tungsten pinhole (b) was observed even at maximum power (880W). The ZrO_2-coated stainless-steel pinhole sustained greater average power than the uncoated stainless-steel pinhole, with the onset of burning observed at 570 W (c). At some point (average power way above the kW regime), a single WL10 pinhole is likely to face melting issue as well and schemes based on double slits (stretching out the heated area to two successive lines instead of a single focal point) might be required [8].

Figure 6 (b) illustrates that the surrounding lobes impact the pinhole mount significantly. To prevent this, a 45° holed mirror is introduced on the converging composite beam in its way to the coherent combination (d). The 13 mm mirror hole diameter is located 50 cm before the pinhole. Unwanted beams are directed towards a dedicated beam dump consisting of a reservoir with circulating water. A window with appropriate antireflective coating ensures an efficient coupling into the water (absorption coefficient at 1 µm is $\alpha \sim 20\ m^{-1}$). Such a beam dump allows efficient average power management while eliminating the creation of dust particles at a laser-solid interface (as on solid beam dumps). Dumping these beams is not the only possibility; a two-step CBC [9] scheme has been envisioned, where these six beams that are already in phase are coherently added, offering a second beam to users.

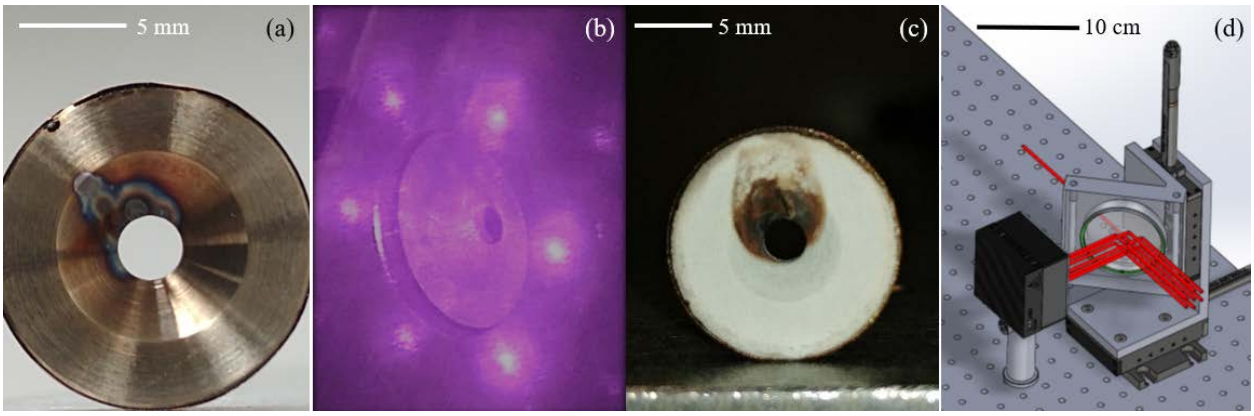

Figure 6. (a) Stainless steel pinhole with the onset of melting at 440 W average power operation; (b) impact of surrounding lobes on W pinhole mount; (c) ZrO_2 coated pinhole; (d) CAD view illustrating surroundings beams deviation toward a beam dump.

3. Average power adjustment at constant peak power

The XCAN front end relies on an oscillator delivering nJ pulses at 55 MHz. Three acousto-optic modulators are inserted as pulse pickers to reduce the repetition rate. XCAN laser amplifiers are CW pumped at 976 nm with up to 60 W per amplifier. Consequently, a decrease in repetition rate implies a proportional increase in pulse energy. At lower repetition rates, typically a few hundred kHz, the output energy per channel reaches values that do not allow efficient operation of the laser system. Above 75 µJ, a 2.5 ns pulse amplified through the 1.6 m long silica fiber with a 30 µm diameter mode accumulates a significant nonlinear phase ($\gg$3 rad). The XCAN servo loops can compensate phase and delay perturbations (thermal drifts, mechanical vibrations, acoustic noises, …) from channel to channel up to a 400 Hz effective bandwidth and then efficiently keep coherence between them. However, nonlinear phase variations are almost instantaneous (they occur on the fs scale) and cannot be corrected. It is therefore mandatory to operate in an energy regime that does not lead to excessive B-integral (up to 5–6 rad). Typically, the XCAN operating

repetition rate is set at 333 kHz. With a 1 mJ pulse, this leads to 333 W average power, and 300 fs compressed pulses lead to 3 GW peak power.

Certain experimental configurations and applications require decoupling average from peak power adjustment. High repetition rate operation can induce thermal effects that obscure both the observation and analysis of a specific high peak power phenomenon (*e.g.*, nonlinear effects). One can also consider experiments involving several laser beams (pump-probe) and/or relying on evolving targets (gas, liquid, droplet jets), where nominal peak power is necessary without the nominal pulse repetition rate. Also, the motivation for decoupling occurs in the area of materials processing where one may want to use a single pulse or a tailored burst of pulses to perform some material processing task, such as drilling a small hole or removing the surface to a set depth.

Deriving a technical solution to adjust the pulse repetition of the laser while keeping a nominal peak power appears therefore beneficial for such research and industrial needs.

A Pockels cell can select a single pulse from a MHz pulse train (in the XCAN nominal configuration pulses are separated by 3 µs), but the electro-optic crystal (*e.g.*, KD*P, KTP, BBO, $LiNbO_3$) at the core of such optical switch suffers from residual absorption leading to internal temperature rise degrading the quality of the transmitted laser polarization adjustment as well as beam quality. Properly designed BBO Pockels cells can sustain several hundred W of average power, but large aperture (>10 mm) BBO crystals are costly and two of them must be used in series to lower the drive voltage to a realistic value. Even so, two 10 x 10 x 20 mm^3 crystals in series still have a half-wave voltage of approximately 11.3 kV. A KD*P Pockels cell prototype was operated at kW average power [10] thanks to an efficient but rather complex cooling architecture: a continuous flow of helium is circulating through four slices of crystal, an approach not suitable for most users.

We opted therefore for a KD*P crystal-based Pockels cell from Leysop (EM510M series), which is an order of magnitude less expensive (even not considering the additional cost of second Pockels cell driver) than a BBO cell. Transmission of dielectrically coated BBO faces and windows are respectively 99.7% and 99.6% over a 970-1100 nm bandwidth. Knowing that a typical KD*P crystal-based Pockels cell can operate efficiently up to a few W of average power at a 1 µm wavelength, a complementary solution is needed when dealing with several hundreds of W. For that purpose, we have developed a homemade chopper with a 2.5% transmission ratio, which is placed upstream from the Pockels cell. Standard metallic choppers cannot be used since they are unable to sustain absorption at a level of hundreds of Watts. A partially reflective rotating wheel is used instead. To minimize any vibration imprinted on the laser beam, the chopper reflects the unwanted fraction of the incoming pulse train, while the burst of pulses used for experiments is transmitted through the chopper. To avoid potential air turbulence impacting a beam passing through any angularly cut fast rotating mirror [11], we use a highly reflective/antireflective coated fused silica disk according to the design displayed in Figure 7. Naneo Precision IBS coatings GmbH optimized the coatings with T>99.5% (AR) and R>99.5% (HR) over a 970-1100 nm bandwidth.

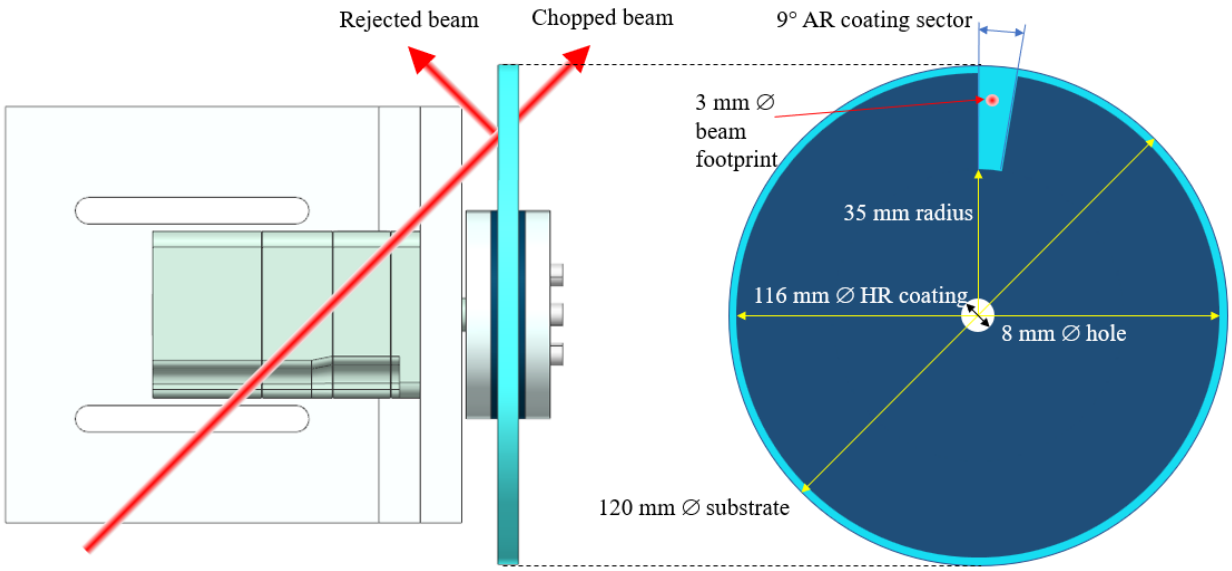

Figure 7. AR/AR coated 9° angular segment in an AR/HR 120 mm diameter disk.

The motor (Yaskawa S7) maximum rotation rate is set at 6000 rpm. At this repetition rate (100 Hz), each 10 ms, a 250 µs long burst containing 82 pulses separated by 3 µs (at the laser repetition rate of 333 kHz) is transmitted by the chopper. At 10 Hz, the 2.5 ms long bursts are separated by 100 ms and contain 825 pulses. Whatever the rotating speed, the average power is reduced to 9°/360°=2.5% of the incident power. For instance, a 165 W average power 333 kHz pulse train carries a 4 W average power when reaching the Pockels cell. Figure 8 displays the linearly polarized pulse sequences entering the Pockels cell when the laser is operated at 333 kHz and the mirror rotation set at 31 Hz. A Thorlabs DET08CFC 5 GHz photodiode is used to record the pulse train. Leading and falling front slopes are related to the beam transverse shape (gaussian), size (3 mm at $1/e^2$), radial position (50 mm from center), and mirror rotating rate (31 Hz). Negative and positive overshoots are related to the photodiode operation.

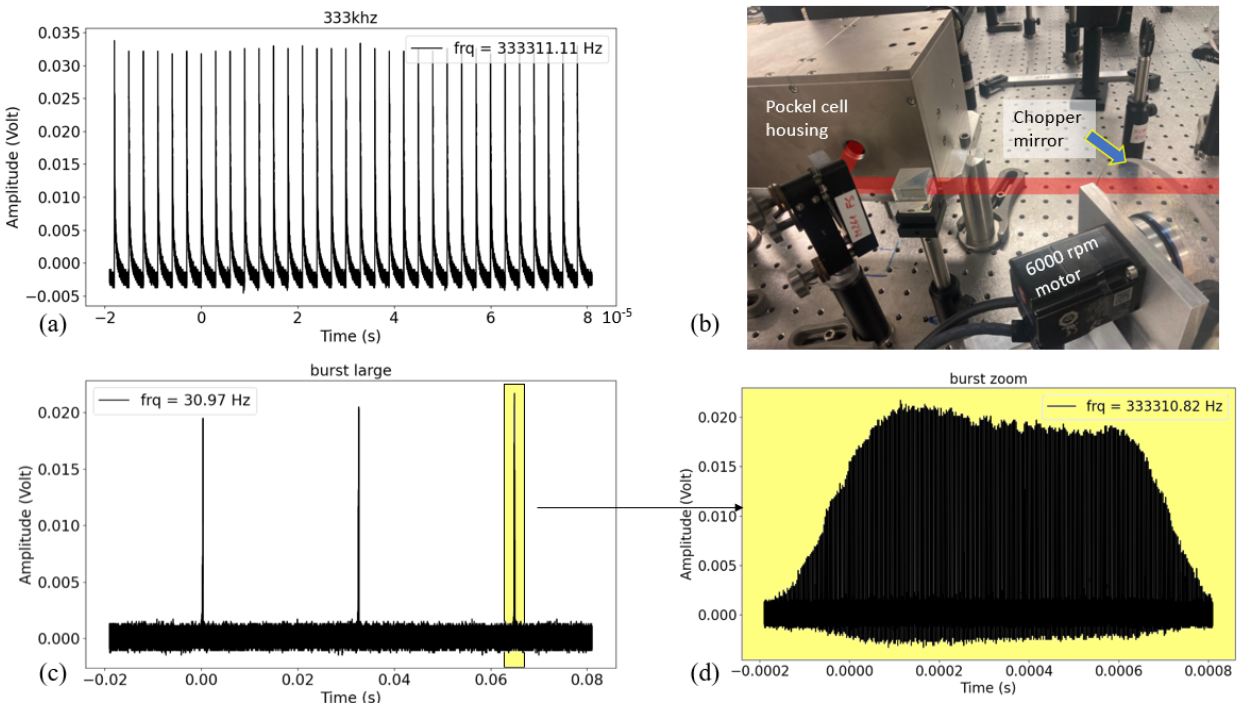

Figure 8. (a) Pulse train within the burst at 333kHz; (b) motor and mirror assembly (front right) and Leysop 1000:1 extinction ratio Pockels cell housing (back left); (c) 31 Hz burst train; and (d) single burst.

Figure 9 displays the Pockels cell output pulse train when applying a 111 µs, 7 kV voltage square signal onto the Pockels cell electrodes. A series of 37 pulses (still 3 µs spaced) have then been selected out of each burst as illustrated in Figure 8 (bottom right). Figure 10 shows a single pulse selection with a 200 ns, 7 kV voltage square signal. Extracting a single pulse from each burst produces pulse trains with repetition rates between 1 and 100 Hz, where the upper limit is set by the maximum chopper rotation rate. All traces have been recorded with a Tektronix MDO34 1 GHz oscilloscope.

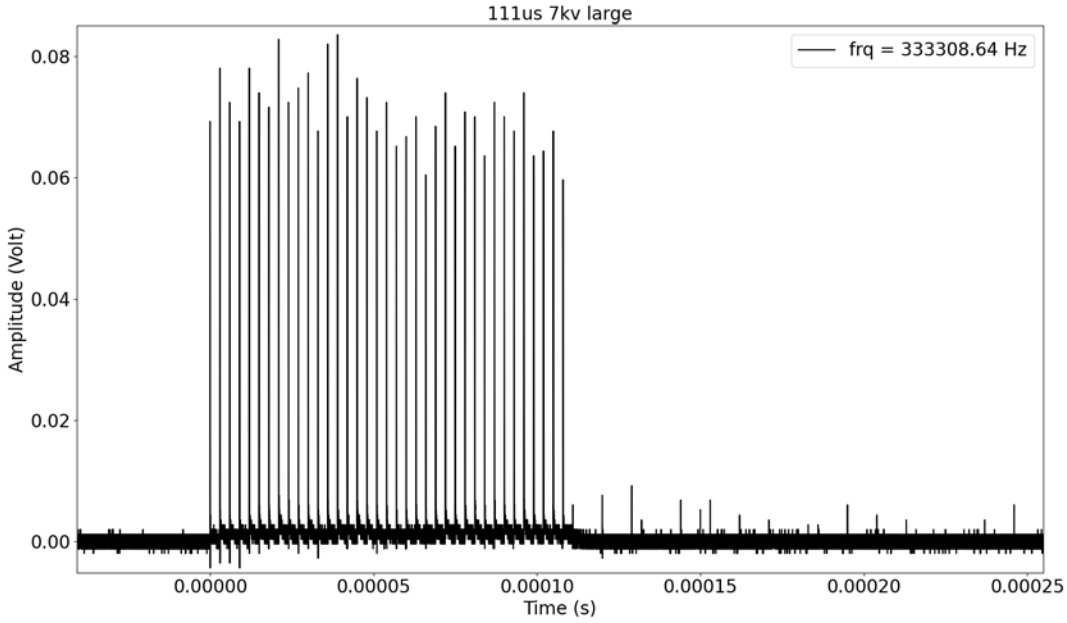

Figure 9. Pockels cell output pulse train recorded with a Thorlabs DET08CFC 5GHz photodiode when applying a 111 µs, 7 kV voltage square signal onto the KD*P electrodes. A series of 37 pulses can be observed. The contrast exceeds 1:100, evaluation being limited by the residual noise level on the photodiode. A few erratic parasitic signals appear on the trailing edge.

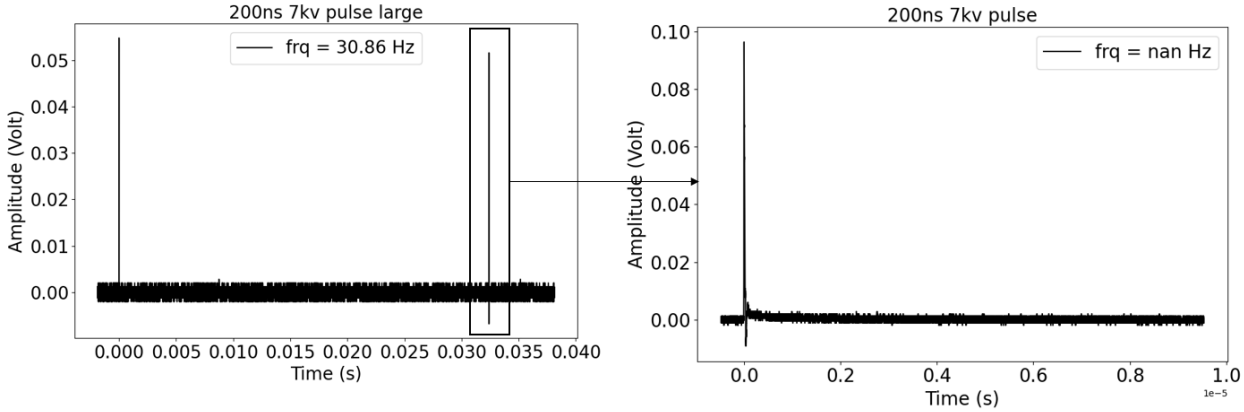

Figure 10: Single pulse extraction from the 31 Hz burst.

CONCLUSION

Thermal management solutions specific for CBC were developed with an additive processed laser head hosting several dozens of fibers and a far-field beam selection with a tungsten pinhole coupled to a holed mirror and a water beam dump. An innovative technical solution was designed, validated, and implemented on XCAN CBC laser to independently manage the peak and average laser power, which is needed for laser-mater interaction applications. The combined use of an optical chopper and a standard Pockels cell addresses that goal while expanding the range of repetition rates made available to users. Altogether, these developments allow a simultaneous kW/GW average/peak powers operation with independent adjustability.

Acknowledgments

The authors would like to thank the Laboratoire Interdisciplinaire Carnot de Bourgogne (https://lermps.utbm.fr/) for depositing zirconium on our steel holes as well as Thales LAS for performing the laser head thermal modeling.

This work received funding from the European Innovation Council (Open grant No. 101047223-NanoXCAN and Horizon 2020 Framework Programme 654148), the Agence de l'Innovation de Défense (AID) and the Centre National des Etudes Spatiales (CNES).
This work was supported in part by the U.S. Department of Defense, Defense Threat Reduction Agency (HDTRA1-20-2-0002).

References

1. C.J. Saraceno, D. Sutter, T. Metzger, and M. Abdou Ahmed, "The amazing progress of high-power ultrafast thin-disk lasers," J. Eur. Opt. Soc.-Rapid Publ. 15(1), 15 (2019). DOI: https://doi.org/10.1186/s41476-019-0108-1
2. I. Fsaifes, L. Daniault, S. Bellanger, M. Veinhard, J. Bourderionnet, C. Larat, E. Lallier, E. Durand, A. Brignon, and J.-C. Chanteloup, "Coherent beam combining of 61 femtosecond fiber amplifiers", Optics Express, 28(14), 20152-20161 (2020). DOI: https://doi.org/10.1364/OE.394031
3. M. Veinhard, S. Bellanger, L. Daniault, I. Fsaifes, J. Bourderionnet, C. Larat, E. Lallier, A. Brignon, J.-C. Chanteloup, "Orbital Angular Momentum beams generation from 61 channels Coherent Beam Combining femtosecond Digital Laser", Optics Letters, Vol. 46, No.1, pp.25-28 (2021). DOI: https://doi.org/10.1364/OL.405975
4. C. Lechevalier, C.-A. Ranély-Vergé-Dépré, I. Fsaifes, R. Becheker, G. Boer, and J.-C. Chanteloup, "Controlled generation of orbital angular momentum beams with coherent beam combining digital laser and liquid-crystal q-plate", IEEE Photonics Journal, Vol. 16, No. 04, 2024. DOI: https://doi.org/10.1109/JPHOT.2024.3421244
5. L. Lavenu, M. Natile, F. Guichard, Y. Zaouter, X. Delen, M. Hanna, E. Mottay, and P. Georges, "Nonlinear pulse compression based on a gas-filled multipass cell", Optics Letters Vol. 43, No. 10, pp. 2252-2255 (2018). DOI: https://doi.org/10.1364/OL.43.002252
6. A. Heilmann , J. Le Dortz, L. Daniault, I. Fsaifes, S. Bellanger, J. Bourderionnet, C. Larat, E. Lallier, M. Antier, E. Durand, C. Simon Boisson, A. Brignon & J.-C. Chanteloup, "Coherent beam combining of seven fiber chirped-pulse amplifiers using an

interferometric phase measurement", Optics Express Vol. 26, No. 24, pp. 31542-31553 (2018). DOI: https://doi.org/10.1364/OE.26.031542

7. I. Fsaifes, C. Ranély-Vergé-Dépré, R. Becheker, K. Fritsch, O. Pronin, and J. Chanteloup, "Post-compression of shaped coherent beam combining femtosecond digital laser pulses," in Laser Congress 2023 (ASSL, LAC), Technical Digest Series (Optica Publishing Group, 2023), paper ATh3A.1. DOI: https://doi.org/10.1364/ASSL.2023.ATh3A.1
8. H. Xiong, X. Yuan, X. Zhang, & K. Zou, "Performance of a simplified slit spatial filter for large laser systems", Optics Express Vol. 22, No. 18, pp. 22211-22219 (2014). DOI: https://doi.org/10.1364/OE.22.022211
9. I. Fsaifes, C-A. Ranély-Vergé-Dépré, M. Veinhard, S. Bellanger & J.-C. Chanteloup, "Far field energy distribution control using a coherent beam combining femtosecond digital laser", Optics Express, Vol. 31, No. 5, pp. 8217-8225 (2023). DOI: https://doi.org/10.1364/OE.474607
10. L. F. Weaver; C. S. Petty; D. Eimerl, "Multikilowatt Pockels cell for high average power laser systems", J. Appl. Phys. 68, 2589–2598 (1990); DOI: https://doi.org/10.1063/1.346483
11. X. Li, T. Scott, C. Cromer, and J. Hadler, "Reflective Optical Chopper Used in NIST High-Power Laser Measurements", J. Res. Natl. Inst. Stand. Technol. 113, 305-309 (2008). DOI: https://doi.org/10.6028/jres.113.024